Inorganic Chemistry

Article

pubs.acs.org/IC

Synthesis and Crystal Structures of $BaLaSi_2$ with cis−trans Si Chains and Ba_5LaSi_6 with Pentagonal Si Rings

Takayuki Hashimoto,[†] Hisanori Yamane,*[,†] Takahiro Yamada,[†] and Takashi Sekiguchi[‡]

[†]Institute of Multidisciplinary Research for Advanced Materials, Tohoku University, 2-1-1 Katahira, Aoba-ku, Sendai 980-8577, Japan

[‡]National Institute for Materials Science, Tsukuba, Ibaraki 305-0044, Japan

Supporting Information

ABSTRACT: Prismatic single crystals of novel compounds $BaLaSi_2$ and Ba_5LaSi_6 were synthesized from the elements with or without a Na flux. The crystal structures of the compounds were analyzed by X-ray diffraction. $BaLaSi_2$, containing cis−trans $^1_\infty$[Si] chains, crystallizes in an orthorhombic cell (a = 4.6414(2) Å, b = 14.8851(7) Å, c = 6.7519(5) Å; space group, *Cmcm* (No. 63), Z = 4) and is isotypic with the low-temperature phase of LaSi. The crystal structure of Ba_5LaSi_6 (a = 17.1447(5) Å, b = 4.8767(1) Å, and c = 17.9102(4) Å; space group *Pnma* (No. 62), Z = 4) is a new type containing isolated anionic groups (^{0}[Si_5−Si]) of a pentagonal Si ring with a Si−Si stem. The electrical resistivities measured for the polycrystalline $BaLaSi_2$ and Ba_5LaSi_6 sintered samples were 0.31 and 0.48 mΩ·cm, respectively, at 300 K and increased with temperature. The Seebeck coefficients of $BaLaSi_2$ and Ba_5LaSi_6 were −7.6 and −11 μV·K^{-1}, respectively, at 296 K.

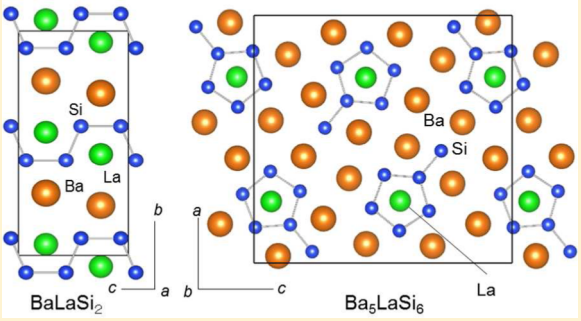

1. INTRODUCTION

Many Zintl compounds composed of alkali, alkaline-earth, and/or rare-earth elements with silicon have been synthesized, and their crystal structures have been elucidated.[1−3] According to the binary phase diagrams,[4,5] the compounds prepared at ambient pressure in the Ba−Si system are Ba_2Si, Ba_5Si_3, BaSi, Ba_3Si_4, and $BaSi_2$, and those in the La−Si system are La_5Si_3, La_3Si_2, La_5Si_4, LaSi, and $LaSi_2$. Electrical properties of $BaSi_2$, BaSi, Ba_3Si_4, LaSi, and $LaSi_2$ have been characterized, and some of them have been investigated for their application as materials for thermoelectric devices and solar cells.[6−13] In the Ba−La−Si ternary system, $Ba_{1-x}La_xSi_2$ ($0 \le x \le 0.08$) solid solutions have been synthesized to improve the thermoelectric properties of $BaSi_2$ by La doping, and a power factor of 4.48 × 10^{-5} W·m^{-1}·K^{-2} at 726 K has been reported for a sample with x = 0.02.[13] As far as the authors know, no other compounds except $Ba_{1-x}La_xSi_2$ ($0 \le x \le 0.08$) have been reported in the ternary system. In the present study, single crystals of novel ternary Zintl compounds $BaLaSi_2$ and Ba_5LaSi_6 were prepared, and their crystal structures were analyzed. Electrical resistivities and Seebeck coefficients of polycrystalline sintered samples of the compounds were measured.

2. EXPERIMENTAL SECTION

2.1. Single Crystal Synthesis and Structure Analysis. Barium (Sigma-Aldrich, 99.99%), lanthanum (Mitsuwa Chemicals, 99.9%), silicon (Kojundo Chemical Laboratory, 99.999%), and sodium (Nippon Soda, 99.95%) were used as starting materials. In an Ar gas-filled glovebox, Ba (1 mmol), La (0.25 mmol), Si (0.5 mmol), Na (3.6 mmol), and Ba (2.0 mmol), La (2.0 mmol), Si (4.0 mmol) were weighed for the preparation of $BaLaSi_2$ and Ba_5LaSi_6 single crystals, respectively, and put into crucibles (inner diameter, 6.5 mm; depth, 18 mm) of polycrystalline sintered boron nitride (99.5%, Showa Dendo). The crucibles were sealed in one-end welded stainless-steel (SUS316) tubes (inside diameter, 10.6 mm; length 70 mm) with stainless-steel caps, and heated in an electric furnace. The temperature was raised to 1173 K (rate, 7.5 K·min^{-1}) and maintained for 2 h, and the crucibles were subsequently cooled to 573 K (rate, −4.2 K·h^{-1}). Below 573 K, the samples were cooled to room temperature by shutting off the electric power to the furnace. The tubes were opened in the glovebox, and the products prepared with Na were washed in liquid NH_3 (>99.999%, Japan Fine Products) to dissolve away the Na flux. Details of the Na extraction procedure have been described previously.[14]

Single crystals were analyzed using wavelength dispersive X-ray detectors of an electron microprobe analyzer (EPMA, JEOL, JXA-8200) with standard samples of BaF_2 (JEOL, 99.9%), SiO_2 (JEOL, 99.99%), and LaB_6 (JEOL, 99.93%). Single crystals for crystal structure analysis were picked up under an optical microscope and sealed in glass capillaries with Ar gas. X-ray diffraction (XRD) data were collected using Mo Kα radiation with a graphite monochromator and an imaging plate on a single-crystal X-ray diffractometer (Rigaku, R-AXIS RAPID-II). Diffraction-data collection and unit-cell refinement were performed by the RAPID-AUTO program.[15] Numerical absorption correction was performed by the NUMABS program.[16] The crystal structure of Ba_5LaSi_6 was solved by the direct method using the SIR2004 program.[17] The crystal parameters were refined by the full-matrix least-squares method on F^2 using the SHELXL-97 program installed with WinGX software.[18,19] The structures were illustrated by the VESTA program.[20] The energy of molecular orbitals and the Si−Si bond overlap populations of a [Si_8] chain and a ^{0}[Si_5−

Received: July 17, 2015
Published: September 3, 2015

DOI: 10.1021/acs.inorgchem.5b01604
Inorg. Chem. 2015, 54, 9188−9194

Si] group were calculated by the DV-Xα method using the SCAT code.[21]

2.2. Preparation of Polycrystalline Sample and Electrical Properties. For the synthesis of $BaLaSi_2$ and Ba_5LaSi_6 polycrystalline sintered bulk samples, the stoichiometric amounts of 2.0, 2.0, and 4.0 mmol and of 3.33, 0.67, and 4.0 mmol of Ba, La, and Si, were, respectively, weighed, placed in Ta boats (Niraco, 99.95%), and sealed in the stainless steel tubes with Ar gas. The starting materials were heated to 1023 K at a rate of 6.2 K·min^{-1}, the temperature being maintained for 2 h. The samples were then cooled in the furnace. The products were pulverized with an agate mortar and a pestle in the glovebox. The obtained powders were pressed into rectangular compacts (14 mm × 3 mm × 4 mm) with a die (molding pressure, ~300 MPa). The compacts placed in the Ta boats were sealed again in the stainless steel tubes with Ar and sintered at 1173 K for 24 h. After the sintered samples had been cooled in the furnace, the tubes were cut open, and the resistivity (ρ) and Seebeck coefficient (S) were measured at 296−473 K in Ar by a direct current four-probe method and by a thermoelectric power (ΔE)−temperature difference (ΔT) method, respectively. The electrical resistivity of the samples was also measured in vacuum in the range from 10 to 296 K. After the measurements, the sintered samples were powdered in the glovebox, and the crystalline phases were confirmed in Ar by powder XRD (Bruker, D2 Phaser, Cu Kα).

3. RESULTS AND DISCUSSION

3.1. Crystal Structure of $BaLaSi_2$. Black columnar single crystals of $BaLaSi_2$ with a size of 0.05−0.20 mm were obtained. The crystals were relatively stable in air for at least a few days. The atomic ratio of Ba/La/Si measured with the EPMA was 26.6(5):24.2(4):49.2(4), which was consistent with the ideal ratio of $BaLaSi_2$. The X-ray reflections could be indexed with the orthorhombic cell parameters a = 4.6414(2) Å, b = 14.8851(7) Å, and c = 6.7519(5) Å. Possible space groups of $Cmc2_1$ and $Cmcm$ were determined by the systematic extinction. The crystal structure of $BaLaSi_2$ could be analyzed with the structure model of the low-temperature (LT) phase of LaSi (orthorhombic, a = 4.5621(2) Å, b = 13.4803(5) Å, c = 6.6259(6) Å; space group, $Cmcm$).[11] In the crystal structure of LT-LaSi, there are two 4c sites (La1 and La2) for La atoms and one 8f site (Si1) for Si atoms. It is difficult to distinguish La and Ba atoms by X-ray diffraction because the scattering powers of both atoms are close. In a model adopted for the structure analysis of $BaLaSi_2$, the La2 site of LT-LaSi was replaced by Ba1 judging from the difference of the interatomic distances discussed in the next paragraph. The $R1$ [$F^2 > 2\sigma$ (all data)] value of the refinement with the model was 0.0188. The results of structure analysis, refined atomic coordinates, and displacement parameters, interatomic distances, and Si−Si−Si bond angles are shown in Tables 1−3 and Supporting Information Table S1. Figure 1 illustrates the projections of the crystal structure of $BaLaSi_2$ on the b−c and a−b planes.

The Si atoms are connected to form cis−trans (ct) Si infinite chains ($^1_\infty$[Si]) in the direction of the c axis, and the cis−trans bends are in the b−c plane. La1 sites of LT-LaSi and $BaLaSi_2$ are at the positions surrounded by the cis-bending Si atoms of the chains, forming [$LaSi_2$] slabs on the a−c plane. La2 sites of LT-LaSi and Ba1 sites of $BaLaSi_2$ are between the slabs (Figure 1). The interatomic distances observed for La1−Si1 (3.1282(9)−3.2360(7) Å) and La2−Si1 (3.1597(7)−3.2247(11) Å) are close in the structure of LT-LaSi.[11] The La1−Si1 distances of $BaLaSi_2$ are 3.1878(10)−3.2221(10) Å and consistent with those of LT-LaSi. However, the Ba1−Si1 distances of $BaLaSi_2$ are 3.4150(10)−3.6827(15) Å and longer than the La1−Si1 distances. The Ba1−Si1 distances are

Table 1. Crystal Data and Refinement Results for $BaLaSi_2$ and Ba_5LaSi_6

chemical formula	$BaLaSi_2$	Ba_5LaSi_6
formula weight M_r, g mol^{-1}	332.43	994.15
temperature T, K	293(2)	293(2)
crystal system	orthorhombic	orthorhombic
space group	$Cmcm$ (No. 63)	$Pnma$ (No. 62)
unit-cell dimension a, Å	4.6414(2)	17.1447(5)
b, Å	14.8851(7)	4.8767(1)
c, Å	6.7519(5)	17.9102(4)
unit-cell volume, V, Å^3	466.47(5)	1497.46(6)
Z	4	4
calculated density, D_{cal}, Mg m^{-3}	4.734	4.410
radiation wavelength λ, Å	0.710 75	0.710 75
crystal form	prism	prism
color	black	silver
absorption correction	numerical	numerical
absorption coefficient μ, mm^{-1}	17.724	16.163
crystal size, mm^3	0.138 × 0.054 × 0.040	0.162 × 0.056 × 0.053
limiting index h	$-5 \le h \le 6$	$-22 \le h \le 22$
k	$-19 \le k \le 19$	$-5 \le k \le 6$
l	$-8 \le l \le 8$	$-22 \le l \le 23$
F_{000}	564	1684
θ range for data collection, deg	4.075−27.389	3.290−27.482
reflections collected/unique	2231/321	14 283/1915
R_{int}	0.0360	0.0498
data/restraints/parameters	321/0/15	1915/0/73
weight parameters, a, b	0.0189, 1.4458	0.0, 0.9609
goodness-of-fit on F^2, S	1.159	1.127
$R1$, $wR2$ (all data)[a]	0.0188, 0.0412	0.0211, 0.0355
$R1$, $wR2$ ($I > 2\sigma(I)$)[a]	0.0179, 0.0410	0.0182, 0.0347
largest diff. peak/hole, $\Delta\rho$, e Å^{-3}	1.054/−1.480	1.108/−1.509

[a] $R1 = \sum||F_o| - |F_c||/\sum|F_o|$. $wR2 = [\sum w(F_o^2 - F_c^2)^2/\sum(wF_o^2)^2]^{1/2}$, $w = 1/[\sigma^2(F_o^2) + (aP)^2 + bP]$, where F_o is the observed structure factor, F_c is the calculated structure factor, σ is the standard deviation of F_c^2, and $P = (F_o^2 + 2F_c^2)/3$. $S = [\sum w(F_o^2 - F_c^2)^2/(n-p)]^{1/2}$, where n is the number of reflections and p is the total number of parameters refined.

Table 2. Atomic Coordinates and Equivalent Isotropic Displacement Parameters (Å^2) for $BaLaSi_2$

atom	site	occ	x	y	z	U_{eq}[a]
Ba1	4c	1	0	0.722 90(3)	1/4	0.016 39(15)
La1	4c	1	0	0.450 65(3)	1/4	0.009 37(14)
Si1	8f	1	0	0.076 17(9)	0.0682(2)	0.0116(3)

[a] $U_{eq} = (\sum_i \sum_j U_{ij}\, a_i^* a_j^*\, \mathbf{a}_i \cdot \mathbf{a}_j)/3$

Table 3. Selected Bond Lengths (Å) and Angle (deg) for $BaLaSi_2$[a]

Si1−Ba1^{iv,v}	3.4150(10) × 2	Si1−La1^{viii,ix}	3.2221(10) × 2
Si1−Ba1^{iii}	3.6827(15)	Si1−Si1^{i}	2.448(3)
Si1−La1^{vi,vii}	3.1878(10) × 2	Si1−Si1^{ii}	2.455(3)
		Si1^{i}−Si1−Si1^{ii}	112.11(7)

[a] Symmetry codes: (i) $-x, -y, -z$; (ii) $x, y, -z + 1/2$; (iii) $-x, 1 - y, -z$; (iv) $x - 1/2, y - 1/2, z$; (v) $x + 1/2, y - 1/2, z$; (vi) $-x - 1/2, -y + 1/2, -z$; (vii) $-x + 1/2, -y + 1/2, -z$; (viii) $x - 1/2, y - 1/2, z$; (ix) $x + 1/2, y - 1/2, z$.

DOI: 10.1021/acs.inorgchem.5b01604
Inorg. Chem. 2015, 54, 9188−9194

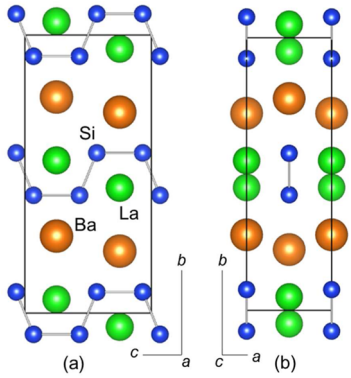

Figure 1. Crystal structure of $BaLaSi_2$ along (a) the *a* axis and (b) *c* axis.

comparable to the Ba−Si distances reported for $BaSi_2$ (3.374−3.766 Å),[22] Ba_3Si_4 (3.309−3.716 Å),[9] BaSi (3.404−3.603 Å),[23] and Ba_5Si_3 (3.376−3.600 Å).[24] The increase of the *b*-axis length is prominent among the changes of the lattice parameters (*a* axis, +1.7%; *b* axis, +10.4%; *c* axis, +1.9%) from LT-LaSi to $BaLaSi_2$. This is also related to the substitution of Ba1 for La2 between the $[LaSi_2]$ slabs.

The Si−Si bond lengths of the ct-$^1_\infty$[Si] chains, which run in the *c*-axis direction in $BaLaSi_2$, are 2.448(3) and 2.455(3) Å and shorter than those of LT-LaSi (2.482(3) and 2.605(3) Å).[11] The Si−Si−Si bond angle of 112.11(7)° in $BaLaSi_2$ is larger than the angle of 108.6° in LT-LaSi, in accordance with the longer *c*-axis length of $BaLaSi_2$.

Figure 2 shows the coordination environment around a silicon chain in $BaLaSi_2$. Si atoms are surrounded by three Ba

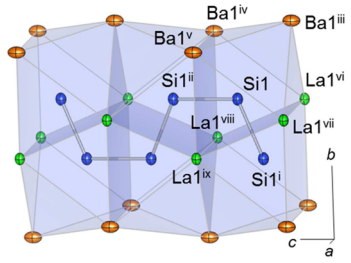

Figure 2. Atomic arrangement around a silicon chain of $BaLaSi_2$. Displacement ellipsoids are drawn at the 75% probability level. Symmetry Codes: (i) $-x, -y, -z$; (ii) $x, y, -z + 1/2$; (iii) $-x, 1 - y, -z$; (iv) $x - 1/2, y - 1/2, z$; (v) $x + 1/2, y - 1/2, z$; (vi) $-x - 1/2, -y + 1/2, -z$; (vii) $-x + 1/2, -y + 1/2, -z$; (viii) $x - 1/2, y - 1/2, z$; (ix) $x + 1/2, y - 1/2, z$.

atoms and four La atoms. Two Ba and four La atoms form a trigonal prism, and one Ba atom is at the cap position above a prism plane, forming a rectangular pyramid (monocapped trigonal prism). The other two noncapped prism planes are shared, and the monocapped trigonal prisms including the ct-$^1_\infty$[Si] chain are aligned in the *c*-axis direction.

3.2. Crystal Structure of Ba_5LaSi_6. The obtained single crystals of Ba_5LaSi_6 were silver, prismatic, 0.1−0.2 mm in length, and unstable in air. The molar ratio, Ba/La/Si = 42.5(5):8.5(4):49.0(5) by EPMA analysis, agreed with the ratio Ba/La/Si = 41.7:8.3:50.0 of Ba_5LaSi_6. The refined lattice parameters are orthorhombic, a = 17.1447(5) Å, b = 4.8767(1) Å, and c = 17.9102(4) Å, and the systematic extinction indicated possible space groups of $Pn2_1a$ and *Pnma*. The crystal structure was analyzed with an $R1$ [$F^2 > 2\sigma$ (all data)] value of 0.0211 using a model derived by the direct method with the higher-symmetry space group of *Pnma* (Table 1). The refined atomic coordinates, displacement parameters, interatomic distances, and Si−Si−Si angles are listed in Tables 4−5 and Supporting Information Table S2.

Table 4. Atomic Coordinates and Equivalent Isotropic Displacement Parameters (Å^2) for Ba_5LaSi_6

atom	site	occ	*x*	*y*	*z*	U_{eq}[a]
Ba1	4*c*	1	0.068 87 (2)	1/4	0.692 06 (2)	0.013 67 (7)
Ba2	4*c*	1	0.076 89 (2)	1/4	0.434 89 (2)	0.014 87 (7)
Ba3	4*c*	1	0.320 55 (2)	1/4	0.768 88 (2)	0.014 45 (7)
Ba4	4*c*	1	0.342 08 (2)	1/4	0.368 47 (2)	0.015 69 (7)
Ba5	4*c*	1	0.471 24 (2)	1/4	0.59331 (2)	0.01378 (7)
La1	4*c*	1	0.251 15 (2)	1/4	0.566 55 (2)	0.009 71 (7)
Si1	4*c*	1	0.046 28 (9)	1/4	0.225 23 (7)	0.0158 (3)
Si2	4*c*	1	0.144 26 (9)	1/4	0.005 07 (7)	0.0121 (3)
Si3	4*c*	1	0.154 96 (8)	1/4	0.140 37 (7)	0.0115 (3)
Si4	4*c*	1	0.289 68 (8)	1/4	0.178 21 (7)	0.0118 (3)
Si5	4*c*	1	0.369 26 (9)	1/4	0.063 02 (7)	0.0123 (3)
Si6	4*c*	1	0.778 25 (9)	1/4	0.544 05 (7)	0.0123 (3)

[a] $U_{eq} = (\sum_i \sum_j U_{ij}\, a_i^* a_j^*\, \boldsymbol{a}_i \cdot \boldsymbol{a}_j)/3$.

Table 5. Selected Bond Lengths (Å) and Angles (deg) for $BaLaSi_2$

Si1−Ba5	3.4085(9) × 2	Si5−Ba2	3.5601(15)
Si1−Ba3	3.4306(11) × 2	Si6−La1	3.1817(8) × 2
Si1−Ba1	3.4696(10) × 2	Si6−Ba3	3.4281(13)
Si1−Ba2	3.7917(14)	Si6−Ba2	3.5008(11) × 2
Si1−Ba4	3.8824(16)	Si6−Ba4	3.5576(11) × 2
Si2−La1	3.2207(9) × 2	Si1−Si3	2.4044(19)
Si2−Ba5	3.4502(14)	Si2−Si3	2.4303(17)
Si2−Ba4	3.4620(9) × 2	Si3−Si4	2.407(2)
Si2−Ba5	3.5164(10) × 2	Si4−Si5	2.4733(18)
Si3−La1	3.2070(9) × 2	Si5−Si6	2.4724(19)
Si3−Ba5	3.3672(10) × 2	Si6−Si2	2.460(2)
Si3−Ba3	3.3792(9) × 2		
Si4−La1	3.2304(8) × 2	Si6−Si2−Si3	106.63(7)
Si4−Ba1	3.4479(10) × 2	Si1−Si3−Si2	124.87(8)
Si4−Ba3	3.4863(10) × 2	Si1−Si3−Si4	124.45(7)
Si4−Ba4	3.5241(13)	Si2−Si3−Si4	110.68(7)
Si5−La1	3.1955(10) × 2	Si3−Si4−Si5	107.13(6)
Si5−Ba2	3.4734(9) × 2	Si4−Si5−Si6	107.39(7)
Si5−Ba1	3.5230(9) × 2	Si5−Si6−Si2	108.18(6)

As shown in Figure 3 and Table 4, all atoms are at the sites of 4*c* and on the *a*−*c* plane at y = 1/4 and 3/4. Six silicon atoms form an isolated anionic group ^{0}[Si_5−Si] composed of a pentagonal ring of Si2−Si6 and a stem of Si1 connected with Si3 of the ring. The La1 site is located at a 10-fold coordination site between the pentagonal ring of Si atoms with La1−Si interatomic distances of 3.1817(8)−3.2304(8) Å (Table 5). The distances almost agree with the distances of La−Si in $BaLaSi_2$ and LT-LaSi and are shorter than the Ba−Si distances of 3.3672(10)−3.8824(16) Å in Ba_5LaSi_6.

Figure 4 shows the atomic arrangement around the Si atoms. The Si1 site is surrounded by eight Ba atoms, six of which form a trigonal prism, and two of which cap two prism planes (dicapped trigonal prism). Si atoms at Si2 and Si4−Si6 sites are coordinated by five Ba and two La atoms, forming [Ba_4La_2]

DOI: 10.1021/acs.inorgchem.5b01604
Inorg. Chem. 2015, 54, 9188−9194

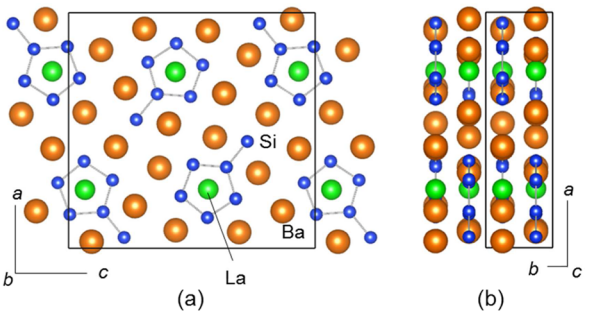

Figure 3. Crystal structure of Ba_5LaSi_6 along (a) the *b* axis and (b) *c* axis.

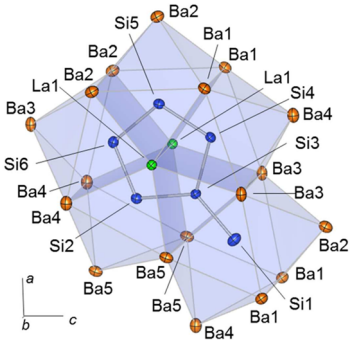

Figure 4. Atomic coordination around $[Si_5{-}Si]$ ring-stem of Ba_5LaSi_6. Displacement ellipsoids are drawn at the 75% probability level.

trigonal prisms having a prism plane capped with a Ba atom (monocapped trigonal prism). Si3 sites are in the trigonal prism of four Ba atoms at Ba3 and Ba5 sites and two La atoms at the La1 site. All prism planes of the trigonal prism are shared with the neighboring dicapped trigonal prism and monocapped trigonal prisms.

3.3. Si−Si Bonding. Postulating the cationic charge of Ba and La atoms to be +2 and +3, the structure formula of $BaLaSi_2$ can be represented as $[Ba^{2+}][La^{3+}][Si_2^{5-}]$, and the average anionic charge of Si is −2.5. LT-LaSi (*Cmcm*),[11] $Li_2La_2Si_3$,[25] $Li_{0.9}Mg_{0.1}BaSi_2$,[26] $LiMgSr_2Si_3$,[27] $LiBaSi_2$, $Li_{0.8}Mg_{0.2}BaSi_2$, $LiSrSi_2$, and $Li_{0.7}Mg_{0.3}SrSi_2$[28] have been previously reported as compounds containing $^1_\infty[Si]$ chains with cis and trans bendings similar or related to the ct-$^1_\infty[Si]$ chains in $BaLaSi_2$. Table 6 summarizes the average M−Si distances (d_{M-Si}), where M (= La, Sr, Ba) atoms are at the cis sites of the ct-$^1_\infty[Si]$ chains, the average Si−Si distances (d_{Si-Si}), and the formal average charges of Si (z) calculated from the formulas of the compounds. The d_{M-Si} increases with increasing atomic radius in the order of La (r_{La}, 1.871 Å) < Sr (r_{Sr}, 2.148 Å) < Ba (r_{Ba}, 2.215 Å).[29] The d_{Si-Si} tends to be longer by an increase in the absolute value of the Si formal charge and does not mainly depend on the M radius.

Since the Si atoms have two bonds in the ct-$^1_\infty[Si]$ chain, the anionic charge of Si atoms is −2 by conventional counting of Zintl polyanions. The Si−Si bond lengths of ct-$^1_\infty[Si]$ chain (2.366(2) and 2.408(2) Å) observed for $Li_{0.9}Mg_{0.1}BaSi_2$ are shorter than the Si−Si length of 2.51(7) Å observed for BaSi (the formal charge of Si, −2).[23,26] The formal charge of Si in $Li_{0.9}Mg_{0.1}BaSi_2$ is −1.55 and between −1 and −2. Wengert and Nesper cited the partial-double bond character as the reason for the shorter bond lengths.[26] Si−Si bond lengths of 2.447−2.506 Å (average, 2.483 Å) have been reported for the cis−trans−trans−trans (cttt) $^1_\infty[Si]$ chains of $Sr_{1.19}La_{0.81}Si_2$.[30] Leoni has discussed the Si−Si bond lengths by partial occupation of σ^* orbitals of the $^1_\infty[Si]$ chain.[30]

Figure 5 shows the molecular orbital energies and overlap population of Si−Si bonding, calculated for the ct-$[Si_8]$ finite chain cut from the structure of $BaLaSi_2$. With an increasing number of electrons in the Si atom from $Si^{2.0-}$ ($Li_2La_2Si_3$) to $Si^{2.5-}$ ($BaLaSi_2$) and $Si^{3.0-}$ (LaSi), the electrons occupy antibonding orbitals, corresponding to the increase of the Si−Si bond length (Table 6).

According to the Zintl−Klemm concept, the formal charges of Si atoms of the isolated $^0[Si_5{-}Si]$ ring stem in Ba_5LaSi_6 are −2 for Si2, Si4, Si5, and Si6 with 2 bonds, −1 for Si3 with three bonds, and −3 for Si1 with one bond. The total charge of $^0[Si_5{-}Si]$ and the average formal charge per Si atom are −12 and −2, respectively, although those are −13 and −2.167 calculated from the formula of Ba_5LaSi_6.

Zintl polyanions of Si pentagonal rings, $^0[Si_5]^{6-}$ and $^0[Si_5]^{7-}$, are contained in Li_8MgSi_6 and $Li_{12}Si_7$, respectively.[31,32] Hexagonal rings of $^0[Si_6]^{10-}$ were found in $Li_2Ba_4Si_6$ and

Table 6. Chemical Formulae, Structural Formulae, Atoms (M = Li, Sr, La, Ba) at *cis*-Sites or Ring Sites, Average Bond Lengths (Å) of M−Si (d_{M-Si}) and Si−Si (d_{Si-Si}), and Si formal charges (z) in $Li_2La_4Si_3$, $BaLaSi_2$, LT-LaSi, $Sr_{1.19}La_{0.81}Si_2$, $LiSrSi_2$, $Li_{0.7}Mg_{0.3}SrSi_2$, $LiMgSr_2Si_3$, $LiBaSi_2$, $Li_{0.9}Mg_{0.1}BaSi_2$, $Li_{0.8}Mg_{0.2}BaSi_2$, $Li_{12}Si_7$, Li_8MgSi_6, Ba_5LaSi_6, $Li_2Sr_4Si_6$, and $Li_2Ba_4Si_6$

chemical formula	structural formula	M	d_{M-Si} (Å)	d_{Si-Si} (Å)	z	ref
$Li_2La_2Si_3$	$[Li^{1+}]_2[La^{3+}]_2[Si^{4-}][(Si_2)^{4-}]$	La	3.107	2.386	−2	25
$BaLaSi_2$	$[Ba^{2+}][La^{3+}][(Si_2)^{5-}]$	La	3.205	2.452	−2.5	this study
LT-LaSi	$[La^{3+}][Si^{3-}]$	La	3.209	2.544	−3	11
$Sr_{1.19}La_{0.81}Si_2$	$[Sr^{2+}]_{1.19}[La^{3+}]_{0.81}[(Si_2)^{4.81-}]$	La/Sr	3.190	2.483	−2.41	30
$LiSrSi_2$	$[Li^{1+}][Sr^{2+}][(Si_2)^{3-}]$	Sr	3.315	2.36	−1.5	28
$Li_{0.7}Mg_{0.3}SrSi_2$	$[Li^{1+}]_{0.7}[Mg^{2+}]_{0.3}[Sr^{2+}][(Si_2)^{3.3-}]$	Sr	3.307	2.378	−1.65	28
$LiMgSr_2Si_3$	$[Li^{1+}][Mg^{2+}][Sr^{2+}]_2[Si^{3.14-}][(Si_2)^{3.86-}]$	Sr	3.324	2.383	−1.93	27
$LiBaSi_2$	$[Li^{1+}][Ba^{2+}][(Si_2)^{3-}]$	Ba	3.439	2.377	−1.5	28
$Li_{0.9}Mg_{0.1}BaSi_2$	$[Li^{1+}]_{0.9}[Mg^{2+}]_{0.1}[Ba^{2+}][(Si_2)^{3.1-}]$	Ba	3.442	2.387	−1.55	26
$Li_{0.8}Mg_{0.2}BaSi_2$	$[Li^{1+}]_{0.8}[Mg^{2+}]_{0.2}[Ba^{2+}][(Si_2)^{3.2-}]$	Ba	3.439	2.399	−1.6	28
$Li_{12}Si_7$	$[Li^{+}]_{24}[(Si_4)^{10-}][(Si_5)^{7-}]_2$	Li	2.948	2.368	−1.4	32
Li_8MgSi_6	$[Li^{+}]_8[Mg^{+}][Si^{4-}][(Si_5)^{6-}]$	Li	2.966	2.364	−1.2	31
Ba_5LaSi_6	$[Ba^{2+}]_5[La^{3+}][(Si_6)^{13-}]$	La	3.207	2.449	−2.167	this study
$Li_2Sr_4Si_6$	$[Li^{+}]_2[Ba^{2+}]_4[(Si_6)^{10-}]$	Sr	3.283	2.378	−1.667	34
$Li_2Ba_4Si_6$	$[Li^{+}]_2[Ba^{2+}]_4[(Si_6)^{10-}]$	Ba	3.400	2.382	−1.667	33

DOI: 10.1021/acs.inorgchem.5b01604
Inorg. Chem. 2015, 54, 9188−9194

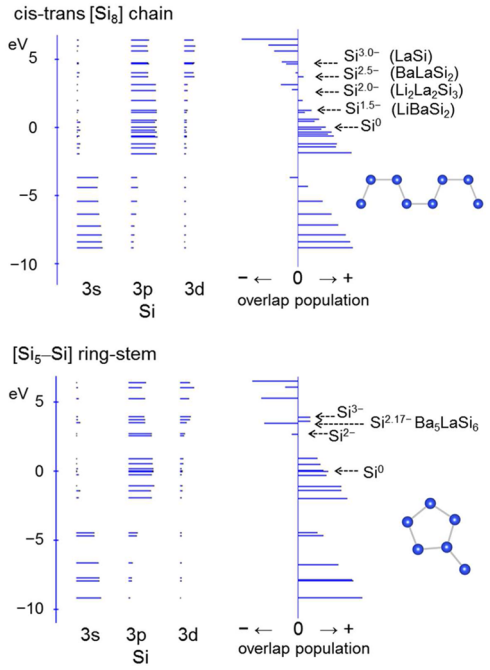

Figure 5. Molecular orbital energy levels and overlap population of Si−Si bonding of $[Si_8]$ chain and $[Si_5–Si]$ ring stem. The energies of the HOMO of the neutral $[Si_8]^0$ chain and $[Si_5–Si]^0$ ring stem are set to 0 eV.

$Li_2Sr_4Si_6$.[33,34] The formal charge of Si atoms by the Zintl−Klemm concept is −2 due to the two bonds for each Si atom in the pentagonal and hexagonal Si rings. However, the formal charges from the formulas of Si atoms in $^0[Si_5]^{6-}$ of Li_8MgSi_6, $^0[Si_5]^{7-}$ of $Li_{12}Si_7$, and $^0[Si_6]^{10-}$ of $Li_2Sr_4Si_6$ and $Li_2Ba_4Si_6$ are −1.2, −1.4, and −1.667, respectively. The average M−Si distance (d_{M-Si}), where there is an M atom (= Li, La, Sr, Ba) at the site between Si rings, average Si−Si distance (d_{Si-Si}), and formal average charge of Si (z) from the chemical formula are also listed in Table 6. The d_{M-Si} increases with increasing M atom radius (r_{Li}, 1.549 Å; r_{La}, 1.871 Å; r_{Sr}, 2.148 Å; r_{Ba}, 2.215 Å).[29] The d_{Si-Si} is longer in the order of Li (d_{Si-Si}, 2.364 Å in Li_8MgSi_6,[31] 2.368 Å in $Li_{12}Si_7$[32]), Sr (d_{Si-S}, 2.378 Å in $Li_2Sr_4Si_6$),[34] Ba (d_{Si-Si}, 2.382 Å in $Li_2Ba_4Si_6$),[33] La (d_{Si-Si}, 2.449 Å in Ba_5LaSi_6). This order corresponds to the electron number or formal charge of Si atoms. The highest occupied molecular orbital (HOMO) calculated for an isolated $^0[Si_5–Si]$ group contained in Ba_5LaSi_6 is antibonding (Figure 5).

A similar Zintl polyanion composed of a pentagonal ring with a stem of Si, $^0[Si_5–Si]^{8-}$, is shown in a figure of reference.[2] However, no information about the composition and crystal structure that contains $^0[Si_5–Si]^{8-}$ was described in that report. To the best of our knowledge, Ba_5LaSi_6 is the first compound to be detected that contains the polyanions of a pentagonal Si ring with a Si stem.

3.4. Electrical Properties. Figure 6 shows powder XRD patterns of the $BaLaSi_2$ and Ba_5LaSi_6 polycrystalline sintered samples prepared for the resistivity measurement. All diffraction peaks of the Ba_5LaSi_6 polycrystalline sintered sample could be indexed with the structure of Ba_5LaSi_6. Small XRD peaks from the high-temperature (HT) phase of LaSi (*Pnma*) were included in the XRD pattern of polycrystalline $BaLaSi_2$ sample. The relative densities of the sintered samples of $BaLaSi_2$ and Ba_5LaSi_6 were 67% and 72%, respectively.

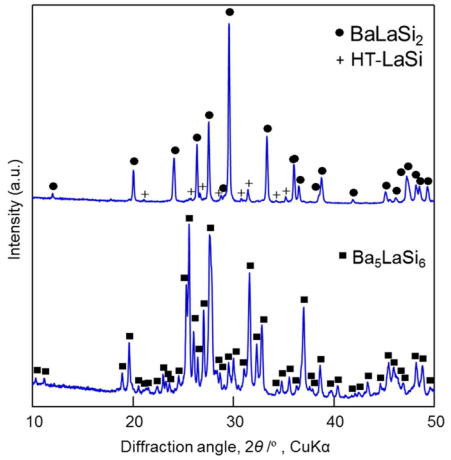

Figure 6. Powder XRD patterns of the $BaLaSi_2$ and Ba_5LaSi_6 polycrystalline sintered samples.

Figure 7 shows the temperature dependence of electrical resistivity measured for the samples of $BaLaSi_2$ and Ba_5LaSi_6.

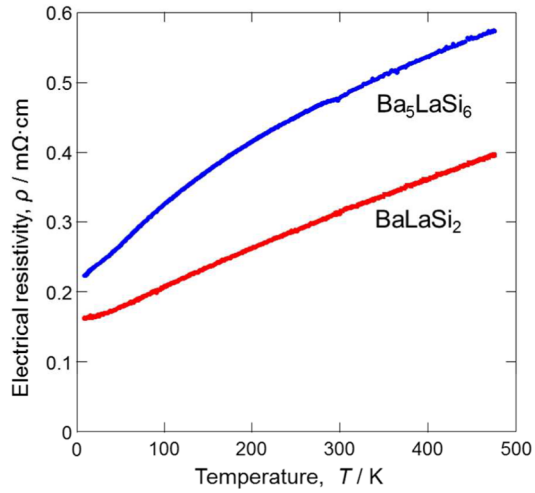

Figure 7. Electrical resistivities of the $BaLaSi_2$ and Ba_5LaSi_6 sintered samples.

The resistivities (ρ) of the $BaLaSi_2$ and Ba_5LaSi_6 sintered samples were 0.31 and 0.48 mΩ·cm, respectively, at 300 K, and increased with increasing temperature, indicating metallic conduction behavior. The resistivities were in the range of those (<0.001−0.38 mΩ·cm) reported at room temperature for BaSi,[8] Ba_3Si_4,[9] HT-LaSi,[10] LT-LaSi,[11] LT-$LaSi_2$, and HT-$LaSi_2$,[12] all of which also exhibit metallic conduction.

The results of Seebeck coefficient measurement are shown in Figure 8. The Seebeck coefficients (S) of the $BaLaSi_2$ and Ba_5LaSi_6 sintered samples were −7.6 and −11 $\mu V \cdot K^{-1}$ at 296 K, respectively, and the absolute values increased with increasing temperature. Such a small S value (almost 0 $\mu V \cdot K^{-1}$ at 331 K) has also been reported for HT-LaSi.[10] $Ba_{1-x}La_xSi_2$ ($0 \le x \le 0.08$) showed semiconducting behavior and had S values of ca. −650 $\mu V \cdot K^{-1}$ at 340 K.[13] The maximum power factors ($S^2 \cdot \rho^{-1}$) of the $BaLaSi_2$ and Ba_5LaSi_6 samples were 2.9×10^{-5} $W \cdot m^{-1} \cdot K^{-2}$ at 475 K and 2.8×10^{-5} $W \cdot m^{-1} \cdot K^{-2}$ at 416 K, respectively, which were ~60% of the power factor (4.48×10^{-5} $W \cdot m^{-1} \cdot K^{-2}$ at 726 K) reported for $Ba_{1-x}La_xSi_2$ (x = 0.02). These power factors are ~2 orders of magnitude lower than those of Bi_2Te_3-

DOI: 10.1021/acs.inorgchem.5b01604
Inorg. Chem. 2015, 54, 9188−9194

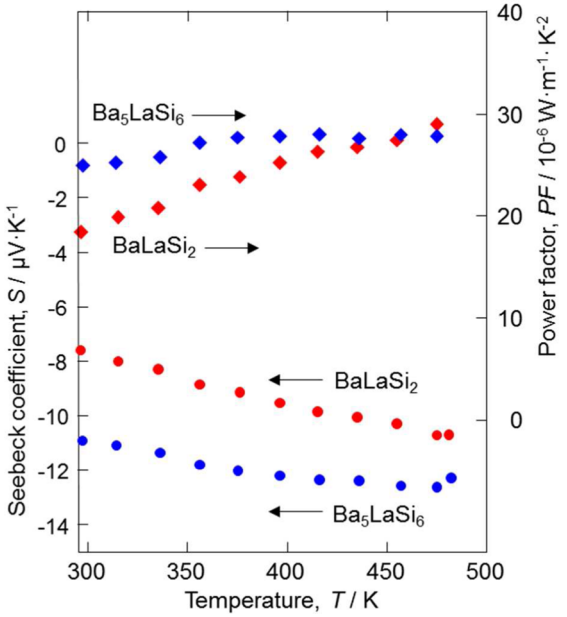

Figure 8. Seebeck coefficients and power factors of the $BaLaSi_2$ and Ba_5LaSi_6 sintered samples.

related materials used for thermoelectric devices. The effect of the HT-LaSi slightly contained in the $BaLaSi_2$ sample could not be clarified.

4. CONCLUSIONS

Two novel ternary orthorhombic compounds, $BaLaSi_2$ (*Cmcm*) and Ba_5LaSi_6 (*Pnma*), were synthesized. $BaLaSi_2$ is isostructural with the LT phase of LaSi, having cis–trans infinite $^1_\infty[Si]$ chains. Isolated anionic groups of $^0[Si_5–Si]^{13-}$ composed of a pentagonal Si ring with a Si stem are contained in the structure of Ba_5LaSi_6. The average Si formal charges of $BaLaSi_2$ and Ba_5LaSi_6 are −2.5 and −2.167, respectively, which are larger than the charges of −2 expected from the Zintl–Klemm concept, suggesting the occupation of electrons in antibonding orbitals of Si–Si bonds. The polycrystalline samples of $BaLaSi_2$ and Ba_5LaSi_6 exhibited metallic conduction behavior.

■ ASSOCIATED CONTENT

Supporting Information

The Supporting Information is available free of charge on the ACS Publications website at DOI: 10.1021/acs.inorgchem.5b01604.

Tables of anisotropic displacement parameters of $BaLaSi_2$ and Ba_5LaSi_6. (PDF)
X-ray crystallographic data of $BaLaSi_2$. (CIF)
X-ray crystallographic data of Ba_5LaSi_6. (CIF)

■ AUTHOR INFORMATION

Corresponding Author

*E-mail: yamane@tagen.tohoku.ac.jp. Phone: (+81)22-217-5813. Fax: (+81)22-217-5813.

Author Contributions

The manuscript was written with contributions of all authors. All authors have given approval to the final version of the manuscript.

Notes

The authors declare no competing financial interest.

■ ACKNOWLEDGMENTS

We are grateful to T. Kamaya for his help in EPMA analysis. This work was supported in part by a Grant-in-Aid for Scientific Research (C; No. 25420701, 2014) from the Ministry of Education, Culture, Sports and Technology (MEXT), Japan, and was performed under the Cooperative Research Program of "Network Joint Research Center for Materials and Devices".

■ REFERENCES

(1) Schäfer, H.; Eisenmann, B.; Müller, W. *Angew. Chem., Int. Ed. Engl.* **1973**, *12*, 694–712.
(2) Nesper, R. *Silicon Chemistry from the Atom to Extended Systems;* Jutzi, P., Schubert, U., Eds.; Wiley-VCH: Weinheim, Germany, 2003; p171–180.
(3) Gärtner, S.; Korber, N. *Struct. Bonding (Berlin, Ger.)* **2011**, *140*, 25–57.
(4) Pani, M.; Palenzona, A. *J. Alloys Compd.* **2008**, *454*, L1–L2.
(5) Bulanova, M. V.; Zheltov, P. N.; Meleshevich, K. A.; Saltykov, P. A.; Effenberg, G.; Tedenac, J.-C. J. *J. Alloys Compd.* **2001**, *329*, 214–223.
(6) Nakamura, T.; Suemasu, T.; Takakura, K.; Hasegawa, F.; Wakahara, A.; Imai, M. *Appl. Phys. Lett.* **2002**, *81*, 1032–1034.
(7) Baba, M.; Watanabe, K.; Hara, K. O.; Toko, K.; Sekiguchi, T.; Usami, N.; Suemasu, T. *Jpn. J. Appl. Phys.* **2014**, *53*, 078004.
(8) Evers, J.; Weiss, A. *Solid State Commun.* **1975**, *17*, 41–43.
(9) Aydemir, U.; Ormeci, A.; Borrmann, H.; Böhme, B.; Zürcher, F.; Uslu, B.; Goebel, T.; Schnelle, W.; Simon, P.; Carrillo-Cabrera, W.; Haarmann, F.; Baitinger, M.; Nesper, R.; von Schnering, H. G.; Grin, Y. *Z. Anorg. Allg. Chem.* **2008**, *634*, 1651–1661.
(10) Hashimoto, K.; Kurosaki, K.; Imamura, Y.; Muta, H.; Yamanaka, S. *J. Appl. Phys.* **2007**, *102*, 063703.
(11) Mattausch, H.; Oeckler, O.; Simon, A. *Z. Anorg. Allg. Chem.* **1999**, *625*, 1151–1154.
(12) Long, R. G.; Bost, M. C.; Mahan, J. E. *Appl. Phys. Lett.* **1988**, *53*, 1272–1273.
(13) Hashimoto, K.; Kurosaki, K.; Muta, H.; Yamanaka, S. *Mater. Trans.* **2008**, *49*, 1737–1740.
(14) Kowach, G. R.; Lin, H. Y.; DiSalvo, F. J. *J. Solid State Chem.* **1998**, *141*, 1–9.
(15) *RAPID-AUTO;* Rigaku Corporation: Tokyo, Japan, 2005.
(16) Higashi, T. *NUMABS—Numerical Absorption Correction;* Rigaku Corporation: Tokyo, Japan, 1999.
(17) Burla, M. C.; Caliandro, R.; Camalli, M.; Carrozzini, B.; Cascarano, G. L.; De Caro, L.; Giacovazzo, C.; Polidori, G.; Spagna, R. *J. Appl. Crystallogr.* **2005**, *38*, 381–388.
(18) Sheldrick, G. M. *Acta Crystallogr., Sect. A: Found. Crystallogr.* **2008**, *A64*, 112–122.
(19) Farrugia, L. J. *J. Appl. Crystallogr.* **1999**, *32*, 837–838.
(20) Momma, K.; Izumi, F. *J. Appl. Crystallogr.* **2008**, *41*, 653–658.
(21) Adachi, H.; Tsukada, M.; Satoko, C. *J. Phys. Soc. Jpn.* **1978**, *45*, 875–883.
(22) Imai, M.; Sato, A.; Kimura, T.; Aoyagi, T. *Thin Solid Films* **2011**, *519*, 8496–8500.
(23) Rieger, W.; Parthé, E. *Acta Crystallogr.* **1967**, *22*, 919–922.
(24) Nesper, R.; Zürcher, F. *Z. Kristallogr.—New Cryst. Struct.* **1999**, *214*, 20.
(25) Langer, T.; Dupke, S.; Eckert, H.; Matar, S. F.; Winter, M.; Pöttgen, R. *Solid State Sci.* **2012**, *14*, 367–374.
(26) Wengert, S.; Nesper, R. *Inorg. Chem.* **2000**, *39*, 2861–2865.
(27) Xie, Q.; Nesper, R. *Z. Kristallogr.—New Cryst. Struct.* **2003**, *218*, 289–290.
(28) Xie, Q. Dissertation, ETH, No. 15626, 2004.
(29) Pauling, L. *J. Am. Chem. Soc.* **1947**, *69*, 542–553.
(30) Leoni, S. Dissertation, ETH, No. 12783, 1998.
(31) Nesper, R.; Curda, J.; von Schnering, H. G. *J. Solid State Chem.* **1986**, *62*, 199–206.
(32) von Schnering, H. G.; Nesper, R.; Curda, J.; Tebbe, K.-F. *Angew. Chem., Int. Ed. Engl.* **1980**, *19*, 1033–1034.

DOI: 10.1021/acs.inorgchem.5b01604
Inorg. Chem. 2015, 54, 9188–9194

(33) von Schnering, H. G.; Bolle, U.; Curda, J.; Peters, K.; Carrillo-Cabrera, W.; Somer, M.; Schultheiss, M.; Wedig, U. *Angew. Chem., Int. Ed. Engl.* **1996**, *35*, 984−986.
(34) Bolle, U.; Carrillo-Cabrera, W.; Peters, K.; Schnering, H. G. v. *Z. Kristallogr.—New Cryst. Struct.* **1998**, *213*, 689.

DOI: 10.1021/acs.inorgchem.5b01604
Inorg. Chem. 2015, 54, 9188−9194